

# Quality factor analysis and optimization of digital filtering signal reconstruction for liquid ionization calorimeters

Marco Delmastro

*European Laboratory for Particle Physics (CERN), CH-1211 Geneva 23,  
Switzerland*

---

## Abstract

The Optimal Filtering (OF) reconstruction of the sampled signals from a particle detector such as a liquid ionization calorimeter relies on the knowledge of the normalized pulse shapes. This knowledge is always imprecise, since there are residual differences between the true ionization pulse shapes and the predicted ones, whatever the method used to model or fit the particle-induced signals. The systematic error introduced by the residuals on the signal amplitude estimate is analyzed, as well as the effect on the quality factor provided by the OF reconstruction. An analysis method to evaluate the residuals from a sample of signals is developed and tested with a simulation tool. The correction obtained is showed to preserve the original amplitude normalization, while restoring the expected  $\chi^2$ -like behavior of the quality factor.

*Key words:* Calorimeters, Signal Processing, Digital Filtering  
*PACS:* 29.40.Vj

---

## 1 Introduction

The signals arising from the ATLAS electromagnetic calorimeter (EMC) [1] are shaped by a bipolar filter, then sampled every 25 ns at the LHC bunch crossing frequency and stored in analog buffers. Upon a positive decision from the level-1 trigger, a limited number of these samples (typically 5) are digitized and acquired. The amplitude and timing information of the shaped signals are determined combining the signal pulse samples with a digital filtering technique commonly called Optimal Filtering (OF) [2]: this method is optimized

---

*Email address:* [Marco.Delmastro@cern.ch](mailto:Marco.Delmastro@cern.ch) (Marco Delmastro).

to minimize the noise contribution to the variance of the reconstructed signal amplitude, while guaranteeing that the latter is an unbiased estimator of the true amplitude.

Alongside the amplitude and timing information, the OF reconstruction is designed to produce a quality factor that should allow the discrimination of pathological signals from regular ones. The normalized OF quality factor obtained from regular signals follows a standard  $\chi^2$  distribution, while spurious signals generate large quality factor values: these signals could in principle be identified and be rejected with a cut on this quantity.

The computation of the Optimal Filtering Coefficients (OFC's) for a given readout cell requires the knowledge of the signal pulse shape and of the (thermal and pileup) noise time autocorrelation [2]. While the latter can be directly measured from dedicated noise calibration runs and minimum bias events, several different approaches have been proposed to predict the ATLAS EMC ionization pulse shapes and their relative amplitudes with respect to the calibration signals used to probe the detector readout properties [3,4,5,6]. The precision of these pulse prediction methods is quoted in terms of the difference between the predicted ionization signal and the observed one, the two pulses being normalized to the same amplitude. The vector of differences computed for each digitized sample is commonly called the *residuals* vector (defined in Equation 1): an accurate prediction method is usually quoted to lead to a difference  $< 1\%$  at the sample closest to the signal peak, and always between  $\pm 2\%$  for the neighboring samples [3,4,5,6].

Assuming that such a precision is achieved for the readout cells of the ATLAS EMC using a given pulse prediction scheme, this work aims to study how the unavoidable presence of the residuals systematically affects the signal amplitude reconstruction and its noise variance (Section 4), as well as the relative quality factor distribution, thus impairing the discriminating power of the latter (Section 5).

A technique to optimize the quality factor without spoiling the initial reconstructed amplitude normalization is developed and tested on a reference cell for different possible distributions of the amplitude, which is proportional to the deposited energy. The same technique proves to be a powerful tool to extract from data the ionization pulse shape (up to a normalization factor) when no previous knowledge – even approximate – of it is available (Section 6).

This technique has been developed in the framework of the ATLAS EMC, but it holds for any other detector readout system that exploits the OF reconstruction of multiple-sampled signals (e.g. the ATLAS Tile hadronic calorimeter [7]).

## 2 Notation and nomenclature

In the following a matricial notation will be used in all calculations,  $N_{\text{samples}}$  being the number of signal samples digitized during the data acquisition, thus the typical size of all vectors and matrices:

- $\mathbf{A}$  matrix of size  $N_{\text{samples}} \times N_{\text{samples}}$
- $A_{ij}$   $(i, j)$ -th entry of matrix  $\mathbf{A}$
- $\mathbf{a}$  vector of size  $N_{\text{samples}}$
- $a_i$   $i$ -th entry of vector  $\mathbf{a}$
- $\mathbf{A}^{-1}$  inverse matrix
- $\mathbf{A}^T$  transposed matrix
- $\mathbf{a}^T$  transposed vector
- $a$  scalar

The following nomenclature is used:

- $\mathbf{h}$  vector of samples of normalized observed ionization signal
- $\mathbf{g}$  vector of samples of normalized predicted ionization signal
- $\mathbf{g}'$  vector of samples of normalized predicted ionization signal derivative
- $\mathbf{a}$  vector of amplitude OFC's computed from  $\mathbf{g}$  (and  $\mathbf{g}'$ , if time constraint is included [2])
- $\mathbf{b}$  vector of time OFC's computed from  $\mathbf{g}$  and  $\mathbf{g}'$ , if time constraint is included
- $\mathbf{r}$  vector of pulse residuals:

$$\mathbf{r} = \mathbf{h} - \mathbf{g} \tag{1}$$

- $\mathbf{s}$  vector of observed ionization signal samples for a given pulse amplitude  $A$ :

$$\mathbf{s} = A\mathbf{h} + \mathbf{n} \tag{2}$$

- $\mathbf{n}$  vector of noise contributions to signal samples, having the properties:

$$\langle \mathbf{n} \rangle = \vec{0} \tag{3}$$

$$\langle \mathbf{n}\mathbf{n}^T \rangle = \mathbf{C} \tag{4}$$

**C** noise covariance matrix:

$$\mathbf{C} = \mathbf{C}^T \quad (5)$$

$$\mathbf{C} = \sigma_n^2 \mathbf{R} \quad (6)$$

**R** weight matrix, built from the noise autocorrelation function:

$$\left(\sigma_n^2 \mathbf{R}\right)^{-1} = \frac{1}{\sigma_n^2} \mathbf{R}^{-1} \quad (7)$$

**I** identity matrix

### 3 Numerical examples

All the equations derived in this work are illustrated using a simulation tool that can generate pulses  $\mathbf{s}$  for a given signal  $\mathbf{h}$ , noise autocorrelation  $\mathbf{R}$  and width  $\sigma_n$ , and a chosen distribution of amplitudes  $A$ . The tool computes OFC's  $\mathbf{a}$  (and  $\mathbf{b}$ ) from a given pulse prediction  $\mathbf{g}$  and noise autocorrelation  $\mathbf{R}_{\text{OFC}}$  (not necessarily equal to the signal noise autocorrelation), and applies them to the generated samples to obtain the corresponding distribution of amplitude estimates  $\tilde{A}$  (and time estimates  $\tau$ ), and the relative quality factors (defined below in Section 5.1).

The test signals  $\mathbf{h}$  and  $\mathbf{g}$  (and their residuals  $\mathbf{r}$ ) used in the simulations are plotted in Figure 1: they correspond to ionization pulse predictions used during the ATLAS EMC Barrel commissioning operations in 2007, namely to the ones corresponding to the middle compartment cells located<sup>1</sup> at  $[\eta_{\text{cell}}, \phi_{\text{cell}}] = [20, 50]$  ( $\mathbf{h}$ ) and  $[\eta_{\text{cell}}, \phi_{\text{cell}}] = [20, 51]$  ( $\mathbf{g}$ ). They have been explicitly chosen to be very similar, in order to mimic an optimal situation in which the pulse prediction largely satisfies the precision criteria mentioned in Section 1.

The numerical examples correspond to the fixed pulse phase illustrated in Figure 1, that corresponds to the typical EMC data taking condition at LHC, when  $N_{\text{samples}} = 5$  and the signals are digitized so that the third sample is

---

<sup>1</sup> The position of ATLAS EMC readout cells is specified by using indexes corresponding to the local granularity in pseudorapidity  $\eta$  and azimuthal angle  $\phi$  [1]. In the case of the middle compartment this is  $\Delta\eta \times \Delta\phi = 0.025 \times 0.025$ , implying:

$$\eta = 0.025 \cdot (\eta_{\text{cell}} + 0.5) \quad (8)$$

$$\phi = 0.025 \cdot (\phi_{\text{cell}} + 0.5) \quad (9)$$

located near the pulse maximum  $\pm 2$  ns. The actual values used in the simulations are tabulated in Table 1.

Figure 2 shows the values of the thermal noise autocorrelation function used to generate the noise affecting the pulses  $\mathbf{s}$ . This is carried out by building the matrix  $\mathbf{R}$  as a Toeplitz matrix based on the relevant autocorrelation function, which in this case was measured in high gain from middle cell at  $[\eta_{\text{cell}}, \phi_{\text{cell}}] = [20, 50]$  during the ATLAS EMC Barrel commissioning operations in 2007. The matrix  $\mathbf{R}_{\text{OFC}}$ , used for computing the OFC's, is based on the measured autocorrelation function from a neighboring cell at  $[\eta_{\text{cell}}, \phi_{\text{cell}}] = [20, 51]$ . The two autocorrelation functions are quite similar, and previous studies have shown that the residuals obtained are insensitive to details of the autocorrelation function. We thus use  $\mathbf{R}_{\text{OFC}}$  and  $\mathbf{R}$  interchangeably. A noise width  $\sigma_n = 5$  ADC counts is used, corresponding to a typical value for a EMC Barrel middle compartment in high gain.

Figure 3 shows the distributions of the amplitudes  $A$  generated for the numerical examples. These amplitudes span the range between 0 and 3000 ADC counts, covering a realistic range of the EMC electronics after the ADC pedestal subtraction. In order to illustrate the effects related to the distribution of the energy deposited in a EMC cell, we present results from a flat distribution, an exponential-like and a Gaussian-like distribution of possible amplitudes  $A$ .

#### 4 Amplitude Estimate Error and Noise Variance Bias

The OF estimate of the signal amplitudes  $A$  given the digitized samples  $\mathbf{s}$  is [2]:

$$\tilde{A} = \mathbf{a}^T \mathbf{s} \quad (10)$$

that can be expanded according to Equation (2) as:

$$\tilde{A} = \mathbf{a}^T (A\mathbf{h} + \mathbf{n}) = A\mathbf{a}^T \mathbf{h} + \mathcal{N} \quad (11)$$

where  $\mathcal{N} = \mathbf{a}^T \mathbf{n}$  is the (reduced) noise contribution to OF amplitude estimate  $\tilde{A}$ , that has variance:

$$\sigma_{\mathcal{N}} = \sigma_n \sqrt{\mathbf{a}^T \mathbf{R} \mathbf{a}} \simeq \sigma_n \sqrt{\frac{1}{\|\mathbf{h}\|^2}} \quad (12)$$

where the last approximation holds for small noise autocorrelation and negligible time jitter, and is exactly true if the noise autocorrelation is null and

the OFC's are not optimized for time jitter.

If the ionization pulse prediction  $\mathbf{g}$  is not perfect ( $\mathbf{g} \neq \mathbf{h}$ , Equation (1)), the OF estimate of the pulse amplitude suffers of a systematic error  $\epsilon = \mathbf{a}^T \mathbf{r}$ :

$$\tilde{A} = A \underbrace{\mathbf{a}^T \mathbf{g}}_1 + A \underbrace{\mathbf{a}^T \mathbf{r}}_\epsilon + \mathcal{N}_\epsilon \quad (13)$$

$$\tilde{A} = A(1 + \epsilon) + \mathcal{N}_\epsilon \quad (14)$$

This error is independent of the pulse amplitude and depends only on the shape and amplitude of the residuals  $\mathbf{r}$ . This property suggests a simple correction: for a given set of OFC's a scale factor (e.g. obtained by in-situ calibration with particles of known mass) would restore the proper scale. In our numerical example  $\epsilon \simeq -0.00158$ : the distributions in Figure 4 confirm that the systematic bias is independent of the amplitude size and distribution. The average values of the distributions of the normalized amplitude differences  $\frac{\tilde{A}-A}{A}$  are the same (within statistical errors) for all the three different forms of the amplitude distribution. The widths of the  $\frac{\tilde{A}-A}{A}$  distributions in Figure 4 differ because of the varying relative impact of the the noise on the pulse amplitude, since:

$$\frac{\tilde{A} - A}{A} = \epsilon + \frac{\mathcal{N}}{A} \quad (15)$$

The larger the amount of small signals in the sample under study, the larger the tails in the  $\frac{\tilde{A}-A}{A}$  distribution.

The use of imperfect OFC's also affects the noise contribution to the OF reconstructed amplitude. The size of this bias can be approximatively estimated using Equation (12), and recalling that  $\mathbf{a} = \frac{\mathbf{g}}{\|\mathbf{g}\|^2}$  in the approximation of negligible noise autocorrelation and when no time constraint is imposed:

$$\begin{aligned} \frac{\sigma_{\mathcal{N}_\epsilon}}{\sigma_{\mathcal{N}}} &\simeq \sqrt{\frac{\|\mathbf{h}\|^2}{\|\mathbf{g}\|^2}} = \sqrt{1 + \frac{2\mathbf{g}^T \mathbf{r} + \|\mathbf{r}\|^2}{\|\mathbf{g}\|^2}} \\ &\simeq \sqrt{1 + 2\epsilon} \simeq 1 + \epsilon \end{aligned} \quad (16)$$

The bias to the minimized variance is of similar magnitude as that found for the signal amplitude.

## 5 Quality Factor Analysis

### 5.1 Definition

A  $\chi^2$ -like quantity  $Q$  is usually computed from the signal samples  $\mathbf{s}$  and the amplitude estimate  $\tilde{A}$ , in order to evaluate the quality of the OF signal reconstruction. For a signal of given amplitude  $A$  a vector  $\mathbf{x}$  of differences is built as:

$$\mathbf{x} = \mathbf{s} - \tilde{A}\mathbf{g} \quad (17)$$

and the quality factor is computed as its squared norm:

$$Q^2 = \mathbf{x}^T \mathbf{x} \quad (18)$$

or, if the noise autocorrelation is taken into account, as:

$$Q^2 = \mathbf{x}^T \mathbf{R}^{-1} \mathbf{x} \quad (19)$$

If the time constraint is imposed during the OFC's computation, a set of time OFC's  $\mathbf{b}$  is obtained, and the time estimator  $\tau$  can be computed from the samples as [2]:

$$\tau = \frac{1}{\tilde{A}} \mathbf{b}^T \mathbf{s} \quad (20)$$

In this case, the vector  $\mathbf{x}$  can be computed as:

$$\mathbf{x} = \mathbf{s} - \tilde{A}(\mathbf{g} + \mathbf{g}'\tau) \quad (21)$$

### 5.2 Properties and Limitations

The vector of differences  $\mathbf{x}$  as defined in (17) can be expanded as:

$$\begin{aligned} \mathbf{x} &= \mathbf{s} - \tilde{A}\mathbf{g} & (22) \\ &= A\mathbf{h} + \mathbf{n} - \mathbf{a}^T (A\mathbf{h} + \mathbf{n}) \mathbf{g} \\ &= A\mathbf{h} + \mathbf{n} - A\mathbf{a}^T(\mathbf{g} + \mathbf{r})\mathbf{g} - \mathbf{a}^T \mathbf{n}\mathbf{g} \\ &= A\mathbf{h} + \mathbf{n} - A\mathbf{g} - A\mathbf{a}^T \mathbf{r}\mathbf{g} - \mathcal{N}\mathbf{g} \\ &= \mathbf{n} - \mathcal{N}\mathbf{g} + A(\mathbf{r} - \epsilon\mathbf{g}) & (23) \end{aligned}$$

If the ionization pulse prediction is perfect ( $\mathbf{h} = \mathbf{g}$ ) the difference vector  $\mathbf{x}$  reduces to:

$$\mathbf{x} = \mathbf{n} - \mathcal{N}\mathbf{g} \tag{24}$$

and its components  $x_i$  are then normally distributed (following the statistical properties of  $\mathbf{n}$  and  $\mathcal{N}$ ) around 0. The variable  $Q_n^2$  (*normalized quality factor*):

$$Q_n^2 = \frac{1}{\sigma_n^2} Q^2 = \frac{1}{\sigma_n^2} \mathbf{x}^T \mathbf{R}^{-1} \mathbf{x} \tag{25}$$

follows then a  $\chi^2$  distribution with  $N_{\text{samples}} - 1$  degrees of freedom (Figure 5). The statistical properties of the normalized  $\chi^2$  distribution can then be used to identify, and optionally reject, distorted signals. For instance in the numerical examples, where  $N_{\text{samples}} - 1 = 4$ , the probability that a signal affected only by noise gives a normalized quality factor larger than 25 is smaller than  $10^{-4}$ : cutting all signals with  $Q_n^2 > 25$  would guarantee a very high efficiency while rejecting a large fraction of spurious signals.

On the other hand, if the pulse prediction is not perfect ( $\mathbf{h} \neq \mathbf{g}$ ) the  $\mathbf{x}$  components are no longer normally distributed, since they all contain a contribution related to the distribution of the pulse amplitude  $A$  (Equation (23)). In this case the  $Q_n^2$  variable defined in Equation (25) no longer follows a normalized  $\chi^2$  distribution, long tails arise in the distributions (Figure 6), and the shape of the normalized quality factor  $Q_n^2$  depends now on the original signal amplitude distribution. In this case the discriminating power of the quality factor is impaired. If in fact the normalized quality factor of strongly distorted signals (e.g. in the rare case of important signal pileup from previous events) is so large ( $\gtrsim 10^3$ ) that even the use of imperfect OFC's would not really affect its rejection capability, there are other categories of spurious signals for which the distortion is smaller, that produce quality factor values comparable to the ones obtained using imperfect OFC's. This is for instance the case of slightly out-of-time signals (Figure 7); of signals affected by noise bursts, when occasionally a large noise spike in the readout electronics coherently distorts the signal positively in one of the samples and negatively in the following one (Figure 8); of large cross-talk from neighboring cells (Figure 9), when a signal similar to the pulse derivative (capacitive cross-talk), and proportional to the energy release around the cell, distorts the pulse [8]. In these conditions, when using perfect OFC's the large quality factor values produced are of a similar magnitude as the ones obtained from regular signals using imperfect OFC's.

Another problem concerns the variability of the quality factor distributions from cell to cell. The residuals may in fact differ from cell to cell due to differences in the properties of the readout channels, as well as the accuracy

of the pulse predictions and OFC calculations for each cell. The distribution of amplitudes also differs from cell to cell, due to the spatial variation of energy deposits, and of the different size and depth of the cells in the detector. Differences in the quality factor distributions complicate cross-comparisons of this quantity for different cells, or the construction of meaningful cumulative distributions.

## 6 Residuals estimation from quality factor components

### 6.1 Pseudo-residuals definition

For a pulse of given amplitude  $A$  a vector  $\mathbf{y}$  can be built as the ratio of the  $\mathbf{x}$  components (17) and the reconstructed amplitude  $\tilde{A}$  (14):

$$\mathbf{y} = \frac{\mathbf{x}}{\tilde{A}} = \frac{\mathbf{n} - \mathcal{N}\mathbf{g} + A(\mathbf{r} - \epsilon\mathbf{g})}{A(1 + \epsilon) + \mathcal{N}} \quad (26)$$

We call *event pseudo-residuals* the component of the  $\mathbf{y}$  vector computed for a given pulse amplitude and noise contribution (i.e., for a given energy deposit and readout condition in the cell, thus for a given event).

If the noise contribution could be ignored for each event ( $\sigma_n = 0$ ,  $\mathbf{n} = \vec{0}$ ,  $\mathcal{N} = 0$ ), this  $\mathbf{y}$  vector would assume a simplified form, independent of the pulse amplitude:

$$\boldsymbol{\Psi} = \frac{\mathbf{r} - \epsilon\mathbf{g}}{1 + \epsilon} \quad (27)$$

We call *average pseudo-residuals* this  $\boldsymbol{\Psi}$  vector, and discuss below (Section 6.3) how and under which conditions the components of  $\boldsymbol{\Psi}$  can be obtained from the distributions of the components of  $\mathbf{y}$ . Note that the average pseudo-residuals are orthogonal to the amplitude OFC's, since:

$$\mathbf{a}^T \boldsymbol{\Psi} = 0 \quad (28)$$

## 6.2 Estimation of residuals and calculation of OFC correction from average pseudo-residuals

The system of linear equations which follows<sup>2</sup> from Equation (27):

$$(1 + \epsilon)\Psi = \mathbf{r} - \epsilon\mathbf{g} \quad (30)$$

$$\Psi + \Psi\mathbf{a}^T\mathbf{r} = \mathbf{r} - \mathbf{g}\mathbf{a}^T\mathbf{r} \quad (31)$$

$$\underbrace{(\mathbf{I} - \mathbf{g}\mathbf{a}^T - \Psi\mathbf{a}^T)}_{\mathbf{H}}\mathbf{r} = \Psi \quad (32)$$

unfortunately cannot be solved to find  $\mathbf{r}$ . In fact the matrix  $\mathbf{H}$  is in general ill-conditioned, and in particular exactly singular, when no noise autocorrelation is present in the system. This property is directly related to the component  $\mathbf{g}\mathbf{a}^T$  reducing the rank of  $\mathbf{H}$ , since:

$$\det(\mathbf{g}\mathbf{a}^T) \simeq 0 \quad (33)$$

for general values of  $\mathbf{r}$ , and exactly null when  $\mathbf{R} = \mathbf{I}$ .

The impossibility to solve system (32) is directly related to the (hopeless) attempt to extract information about  $\mathbf{r}$  from  $\epsilon$  in Equation (31): in fact, given a scalar  $\epsilon$  and a vector  $\mathbf{a}$ , there unfortunately exists a infinite set of vectors  $\mathbf{r}$  that satisfy the relation  $\mathbf{a}^T\mathbf{r} = \epsilon$ .<sup>3</sup> This is an intrinsic limitation of the OF signal reconstruction that cannot be circumvented: by applying the OFC's  $\mathbf{a}$  to the samples  $\mathbf{s}$  when estimating the signal amplitude a part of information about the original pulse  $\mathbf{h}$  is lost.

On the other hand, from Equation (27) it is possible to define a more general class of the vectors  $\mathbf{r}_\lambda$  that satisfy the relation  $\mathbf{a}^T\mathbf{r}_\lambda = \lambda$ :

$$\mathbf{r}_\lambda = (1 + \lambda)\Psi + \lambda\mathbf{g} \quad \lambda \in \Re \quad (34)$$

When any of these  $\mathbf{r}_\lambda$  vectors (34) is used to correct the ionization pulse prediction  $\mathbf{g}$ , the resulting corrected pulse  $\mathbf{g}_c$  is *exactly proportional* to the

<sup>2</sup> Equation (32) exploits the relation:

$$\underbrace{(\mathbf{a}^T\mathbf{b})}_{\alpha \in \Re} \mathbf{c} = \underbrace{(\mathbf{c}\mathbf{a}^T)}_{\mathbf{M} \in \Re^n \times \Re^n} \mathbf{b} \quad (29)$$

<sup>3</sup> Consider for instance the vector:

$$\rho = \left\{ \frac{\epsilon}{a_0}, 0, 0, \dots, 0 \right\}$$

ionization pulse  $\mathbf{h}$  we were aiming for, apart from a scale factor:

$$\mathbf{g}_c^\lambda = \mathbf{g} + \mathbf{r}_\lambda = (1 + \lambda)(\mathbf{g} + \mathbf{\Psi}) = \frac{1 + \lambda}{1 + \epsilon} \mathbf{h} \quad (35)$$

Of course the preferred choice would be  $\lambda = \epsilon$ , but the impossibility of this option has already been discussed. On the other hand, by choosing  $\lambda = 0$  an interesting property of the correction is found: the OFC  $\mathbf{a}_c$  obtained from the corrected pulse  $\mathbf{g}_c^{\lambda=0}$  *preserve the reconstructed signal amplitude normalization* obtained from the original  $\mathbf{a}$  OFC's obtained from the initial pulse prediction  $\mathbf{g}$ . If we let  $\mathbf{a}_h$  represent the OFC's corresponding to the true ionization pulse  $\mathbf{h}$ , we have the following relationship between the corrected and the “true” OFC's:

$$\mathbf{a}_c = (1 + \epsilon) \mathbf{a}_h \quad (36)$$

and then ( $\mathcal{N}_h = \mathbf{a}_h n$ ):

$$\tilde{A}_c = \mathbf{a}_c s \quad (37)$$

$$= (1 + \epsilon) (A \mathbf{a}_h \mathbf{h} + \mathbf{a}_h \mathbf{n}) \quad (38)$$

$$= (1 + \epsilon) A + (1 + \epsilon) \mathcal{N}_h \quad (39)$$

The  $\mathbf{a}_c$  OFC's *correctly compensate for errors in the initial prediction of the ionization pulse shape*, while preserving the amplitude normalization obtained from the original  $\mathbf{a}$  OFC's. When trying to optimize the global cell calibration this certainly represents an advantage. In fact, in order to correct for the effects of material in front of the detector, or to compute the correct global energy scale, the reconstructed signal amplitudes are always multiplied by additional calibration factors obtained *in-situ* from reference data samples (e.g. electrons from  $W^\pm$  and  $Z^0$  decays). In the process of computing these factors with an increasing data sample, and optimizing at the same time the reconstruction of the signal amplitudes, the normalization of the latter is better kept preserved in order not to mix the effects.

Whatever the choice of  $\lambda$  (and thus also for  $\lambda = 0$ ) the use of the corrected OFC's *restores the proper behavior of the quality factor*. In fact the components of the difference vector  $\mathbf{x}_c$ :

$$\mathbf{x}_c = \mathbf{s} - \tilde{A}_c \mathbf{g}_c \quad (40)$$

$$\begin{aligned} &= A \mathbf{h} + \mathbf{n} - \frac{1 + \epsilon}{1 + \lambda} \mathbf{a}_h^T (A \mathbf{h} + \mathbf{n}) \frac{1 + \lambda}{1 + \epsilon} \mathbf{h} \\ &= \mathbf{n} - \mathcal{N}_h \end{aligned} \quad (41)$$

are now correctly normally distributed around 0, and:

$$\frac{1}{\sigma_n^2} Q_c^2 = \frac{1}{\sigma_n^2} \mathbf{x}_c^T \mathbf{R}^{-1} \mathbf{x}_c \quad (42)$$

is guaranteed to follow a  $\chi^2$  distribution with  $N_{\text{samples}} - 1$  degrees of freedom.

### 6.3 From event pseudo-residuals to average pseudo-residuals

The possibility of correcting the OFC's by exploiting Equation (35) is related to the capability of extracting consistent estimators of the average pseudo-residuals  $\Psi$  from the distribution of the event pseudo-residuals  $\mathbf{y}$  as defined in Equation (26).

For a given value of the signal amplitude  $A$  every  $y_i$  is distributed as the ratio of two Gaussian variables with different non-zero means, different variances, and a certain correlation. The  $\mathbf{y}$  vector can in fact be expressed as:

$$\mathbf{y}(A) = \frac{A\mathbf{c} + \mathbf{m}}{Ad + \mathcal{N}} = \frac{\mathbf{c} + \frac{1}{A}\mathbf{m}}{d + \frac{1}{A}\mathcal{N}} \quad (43)$$

where:

$$\begin{aligned} \mathbf{c} &= \mathbf{r} - \epsilon \mathbf{g} \\ d &= 1 + \epsilon \end{aligned} \quad (44)$$

and

$$\mathbf{m} = \mathbf{n} - \mathcal{N} \mathbf{g} \quad (45)$$

The components of the  $\mathbf{m}$  vector are normally distributed around 0 with standard deviation  $\sigma_{\mathbf{m}}$ ,  $\rho(\mathbf{m}, \mathcal{N})$  being the vector of their correlation with the denominator noise factor  $\mathcal{N}$ .

The distribution of such a ratio variable is not necessarily Gaussian, especially in case of noisy measurements. On the other hand under certain assumptions, namely that the denominator of the ratio is very unlikely to become negative:

$$Ad \geq 3\sigma_{\mathcal{N}} \quad (46)$$

the probability distribution of this ratio is exactly known<sup>4</sup> [9,10], and the distribution of each component of  $\mathbf{y}(A)$  for a given value of  $A$  approaches a Gaussian  $G(\langle y_i(A) \rangle, \sigma_{y_i(A)})$  with:

$$\langle \mathbf{y}(A) \rangle \sim \frac{\mathbf{c}}{d} = \mathbf{\Psi} \quad (47)$$

$$\sigma_{\mathbf{y}(A)} \sim \frac{1}{Ad} \sqrt{\sigma_{\mathbf{m}}^2 + \mathbf{\Psi}^2 \sigma_{\mathcal{N}}^2 - 2\rho(\mathbf{m}, \mathcal{N})\sigma_{\mathbf{m}}\sigma_{\mathcal{N}}} \quad (48)$$

Note that the standard deviation  $\sigma_{\mathbf{y}(A)}$  scales as  $\frac{1}{A}$ . The local<sup>5</sup> normality condition (46) for  $\mathbf{y}(A)$  is amply satisfied by:

$$\tilde{A} \geq 3\sigma_n \quad (49)$$

since  $\sigma_n > \sigma_{\mathcal{N}}$  because of the OF noise reduction.

Our specific case is additionally complicated by the fact the amplitude  $A$  in (26) follows its particular distribution  $P(A)$  that is not a priori known and that might change from cell to cell depending on the position in the detector and the event sample selection. The cumulative distributions  $D(y_i|P(A))$  of the event pseudo-residual components  $y_i$ , given a probability distribution function  $P(A)$  for the signal amplitudes and holding the normality requirements (49), are then:

$$D(y_i|P(A)) = \int dAP(A)G(\psi_i, \sigma_{y_i(A)}) \quad (50)$$

While the actual shapes of these  $D(y_i|P(A))$  distributions vary according to  $P(A)$  (and in most cases are definitively non-Gaussian!), it is always true that every  $D(y_i|P(A))$  is symmetric, and that the vector of their means corresponds to the average pseudo-residual vector whatever the initial  $P(A)$ , since:

$$\begin{aligned} \langle D(y_i|P(A)) \rangle &= \int dy_i y_i \int dAP(A)G(\psi_i, \sigma_{y_i(A)}) \\ &= \underbrace{\int dAP(A)}_{\equiv 1} \underbrace{\int dy_i y_i G(\Psi_i, \sigma_{y_i(A)})}_{\equiv \Psi_i \forall A, \text{ Equation (47)}} \\ &= \Psi_i \end{aligned} \quad (51)$$

<sup>4</sup> Additionally, under the hypothesis (46) a transformation exists to compute a derived variable that is exactly Gaussian.

<sup>5</sup> The *local* attribution refers here to the fixed value of the pulse amplitude  $A$ .

It is then possible to estimate the average pseudo-residuals  $\Psi$  as the means of the distributions of the event pseudo-residuals, after having applied the local normality requirements (49) on the events entering the distributions.

The property expressed in Equation (51) is clearly verified in our numerical examples. Figure 10 shows the event pseudo-residual distributions corresponding to the three different functional forms for  $P(A)$ , and built from events passing the tight threshold cut on the reconstructed amplitude  $\tilde{A} > 25 = 5\sigma_n$ . Their shape certainly depends on the initial distribution  $P(A)$  of the signal amplitudes  $A$ , but as expected they are always symmetric, and their means (here evaluated by means of a Gaussian fit to the distributions) correspond in all cases to the average pseudo-residual vector  $\Psi$  as shown in Figure 11, the error bars accounting for the width of the corresponding distribution. It is evident that a distribution for the ratio  $y_i$  corresponding to an amplitude distribution  $P(A)$  with predominately small values of  $A$  (such as the exponential in this example) would have larger tails, as the prevailing contributors to  $D$  are Gaussian distributions of large standard deviation (see Equation (48)).

#### 6.4 Average pseudo-residual estimators as OFC pulse correction

The mean values defined in Equation (51) can be used as estimator of  $\Psi$  to correct the original OFC's via Equation (35), by choosing  $\lambda = 0$  to follow the prescription to preserve the original reconstructed signal amplitudes, as discussed in Section 6. Because of the small size of this correction the variation of the pulse derivative  $\mathbf{g}'$  can safely be neglected, and the original one can be used to compute OFC's optimized for time jitter.

When new OFC's are computed from  $\mathbf{g}_c$ ,  $\mathbf{g}'$  and  $\mathbf{R}$ , and reapplied to the original signal samples  $\mathbf{s}$ , as expected from Equation (39) the reconstructed amplitudes are unchanged, preserving the original normalization (Figure 12). The corrected quality factors follow now a  $\chi^2$ -like distribution, for any initial pulse amplitude distribution (Figure 13).

#### 6.5 Pulse shape estimate with flat filter average pseudo-residuals

The pseudo-residuals correction technique proves also to be a powerful tool to extract from data the ionization pulse shape (up to a normalization factor) when no previous knowledge of it is available, whatever the available signal sample. This technique addresses the relative normalization of the signal samples corresponding to different energy deposits in the readout channel under study.

Let  $\mathbf{u}$  be the normalized vector of size  $N_{\text{samples}}$  with all components of equal magnitude (*flat pulse*):

$$\mathbf{u} = \{1, 1, \dots, 1\} \quad (52)$$

and compute the corresponding  $\mathbf{a}_u$  OFC's (*flat filter*). When they are used to reconstruct the signal amplitude and obtain the pseudo-residuals  $\Psi_u$ , from Equation (35) one gets:

$$\mathbf{u} + \Psi_u = \frac{1}{1 + \epsilon_u} \mathbf{h} \quad (53)$$

that is exactly the ionization pulse  $\mathbf{h}$ , up to the normalization factor  $\frac{1}{1 + \epsilon_u}$  (which, for the reason discussed above, is again bound to remain unknown). Figure 14 shows the distributions of the event pseudo-residuals (biased by 1) when the flat filter is used for the reconstruction of the signals belonging to the example distributions; the vectors of their averages nicely correspond to the original ionization pulse  $\mathbf{h}$  (Figure 15). In our example  $\epsilon_u = -0.412544$ : if this value is used to scale the biased pseudo-residual averages in order to compare them with the true  $\mathbf{h}$ , excellent agreement, ranging from  $\sim 10^{-4}$  (exponential distribution of pulses dominated by small pulses, thus larger pseudo-residual distributions) to  $\sim 10^{-5}$  (flat distribution of pulses, narrower pseudo-residual distributions), is found.

## 7 Summary and Conclusions

The unavoidable presence of residuals in the pulse shape prediction used to compute OFC's is bound to introduce a systematic error in OF amplitude estimates. This systematic error is independent of the pulse amplitude and thus can be easily corrected, absorbing it in a simple scale factor. Its size is maintained small (and even negligible) by the usual requirements on the amplitude and shape of the pulse prediction residuals. On the other hand, even the smallest residuals will introduce a bias in the OF quality factor, impairing its discriminating power.

The mathematical properties of the OF reconstruction do not allow the measurement of the residuals shape and amplitude: this loss of information is an intrinsic property of the OF reconstruction technique itself. It is possible to extract from any data sample an alternative vector of *pseudo-residuals*, that allows the correction of the original pulse shape prediction and obtain the exact ionization pulse shape, apart from an uncertainty in the scale factor that is bound to remain unknown. An ad hoc choice for the normalization

of the pseudo-residuals correction is shown to preserve the original normalization of the reconstructed amplitudes. Given any sample of signals from a readout cell it is always possible to obtain its exact pulse shape from an initial (even imprecise) prediction, while its absolute normalization must be obtained from different sources. The pseudo-residuals correction restores the expected  $\chi^2$ -like behavior of the OF quality factor and its full discriminating power, independent of the initial bias.

The OF reconstruction properties discussed here, and the possibility to obtain an optimal correction for any initial pulse shape prediction, suggest a possible calibration strategy for the ATLAS EMC at the LHC start-up: OFC's are computed exploiting the present best knowledge of the ionization pulse shapes and normalizations, and as soon as enough data is collected to compile reliable distributions of the event pseudo-residuals, this technique is used to optimize OFC's (thus quality factor distributions and noise reductions) without spoiling the initial normalization of the reconstructed amplitudes.

## 8 Acknowledgments

The author is greatly indebted to Prof. W.E. Cleland, who first suggested the possibility of computing a correction to the OFC's that would preserve the initial normalization of the reconstructed amplitudes, and then followed the development of this work with continuous interest, encouragement, and very helpful discussions.

The author also wishes to thank R. Froeschl for the useful discussions and comments. The work presented here has been developed within the ATLAS Liquid Argon Group, and the author thanks all the collaboration members.

## References

- [1] The ATLAS collaboration, Liquid Argon Calorimeter Technical Design Report, Tech. Rep. CERN/LHCC/96-41, CERN (1996).
- [2] W.E. Cleland and E.G. Stern, Signal processing considerations for liquid ionization calorimeter in a high rate environment, NIM A 338.
- [3] L. Neukermans, P.Perrodo and R. Zitoun, Understanding the electromagnetic barrel pulse shapes and the absolute electronic calibration, ATLAS Note ATLAS-LARG-PUB-2001-008.
- [4] D. Prieur, Using Time Convolution Method to compute Optimal Filtering

Coefficients for LARG electromagnetic calorimeter, ATLAS Note ATL-LARG-PUB-2005-001.

- [5] D. Banfi, M. Delmastro and M. Fanti, Cell response equalization of the ATLAS electromagnetic calorimeter without the direct knowledge of the ionization signals, *Journal of Instrumentation* 1 (2006) P08001, DOI: 10.1088/1748-0221/1/08/P08001.
- [6] C. Collard, D. Fournier, S. Henrot-Versill, L. Serin, Prediction of signal amplitude and shape for the ATLAS electromagnetic calorimeter, ATLAS Note ATL-LARG-PUB-2007-010.
- [7] E. Fullana et al., Optimal Filtering in the ATLAS Hadronic Tile Calorimeter, ATLAS Note ATL-TILECAL-2005-001.
- [8] F. Hubaut, B. Laforge, D. Lacour, F. Orsini, Test beam Measurement of the Crosstalk in the EM Barrel Module 0, ATLAS Note ATL-LARG-2000-007.
- [9] R. C. Geary, The frequency distribution of the quotient of two normal variables, *Journal of the Royal Statistical Society* 93 (3).
- [10] D. V. Hinkley, On the ratio of two correlated normal random variables, *Biometrika* 56 (3).

$i$	$h_i$	$g_i$	$r_i$	$R_{0i}$	$a_i$	$b_i$
0	0.04761	0.04873	-0.00111	1	0.14516	-7.2531
1	0.65923	0.67365	-0.01442	0.07108	0.22650	-26.9503
2	0.99769	0.99613	0.00156	-0.15330	0.38105	9.1090
3	0.80987	0.80709	0.00279	-0.29747	0.33019	5.9919
4	0.55451	0.55357	0.00095	-0.10336	0.35092	8.3074

Table 1  
Numerical values used in the simulations.

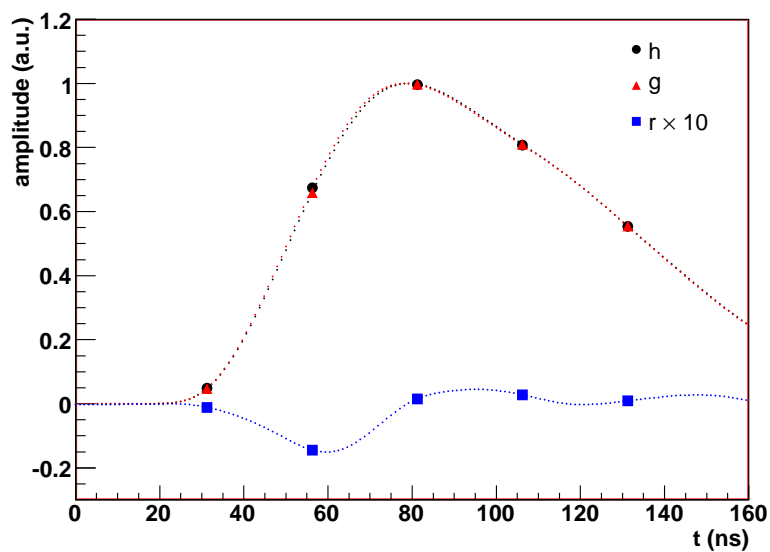


Fig. 1. Signals  $\mathbf{h}$  and  $\mathbf{g}$  and their residuals  $\mathbf{r}$  (magnified by a factor 10) used in the numerical examples.

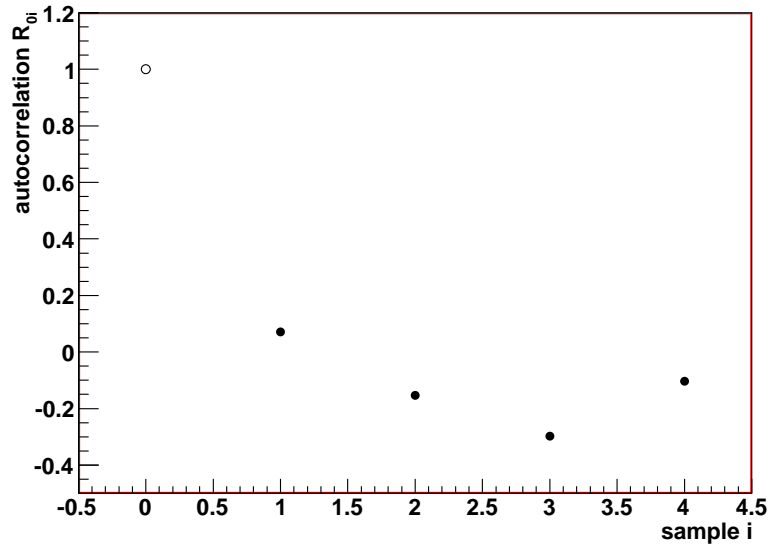


Fig. 2. Noise autocorrelation  $R_{0i} = R_{j0}$  used in the numerical examples.

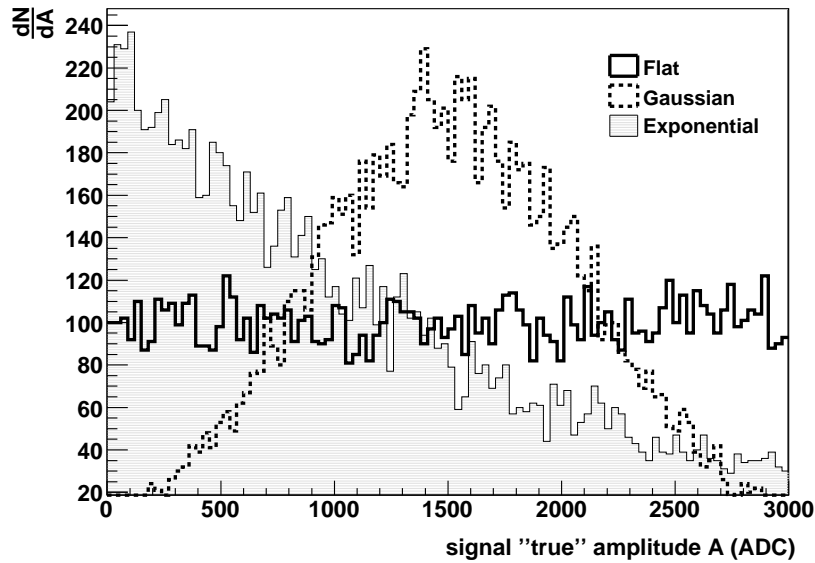


Fig. 3. Distributions of the amplitudes  $A$  generated for the numerical examples.

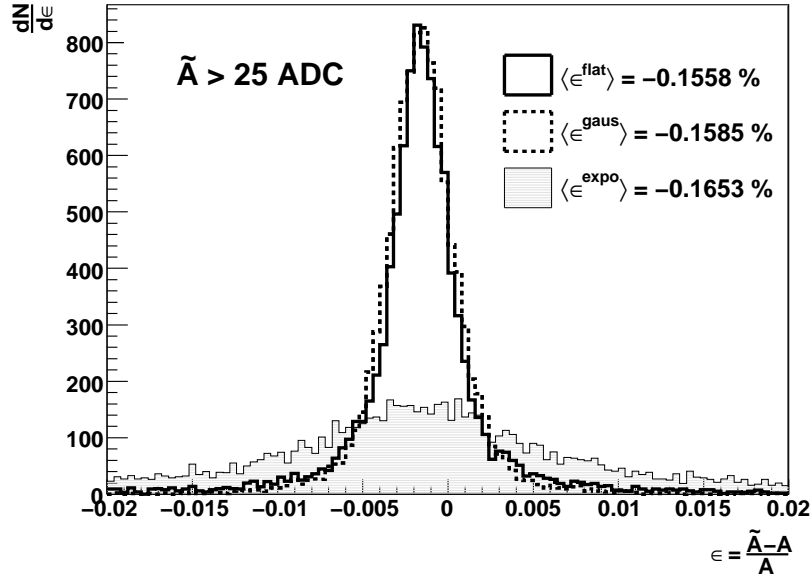


Fig. 4. Distributions of the reconstructed amplitude relative errors, related to the presence of residuals  $\mathbf{r}$  in the pulse used to compute the OFC's.

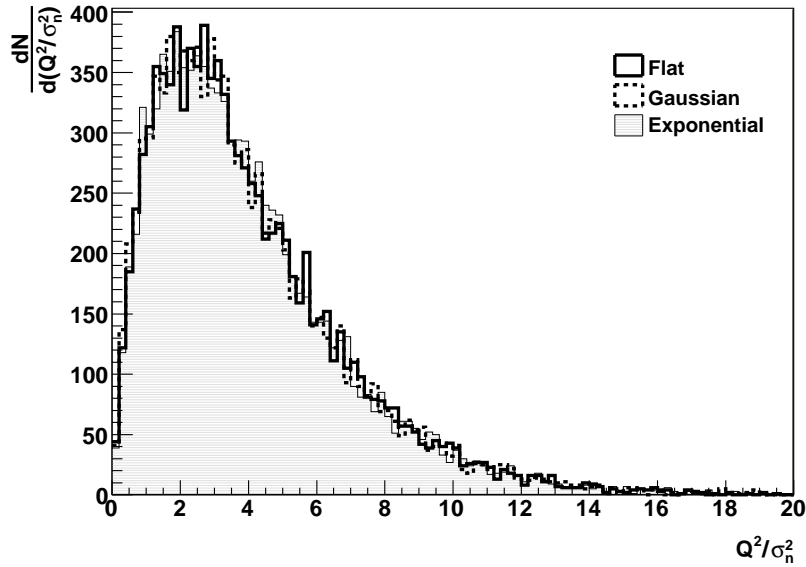


Fig. 5. Quality factor distributions for the different signal amplitudes, as obtained when using perfect OFC's (i.e. computed from the exact ionization pulse  $\mathbf{h}$  for null residuals  $\mathbf{r}$ ).

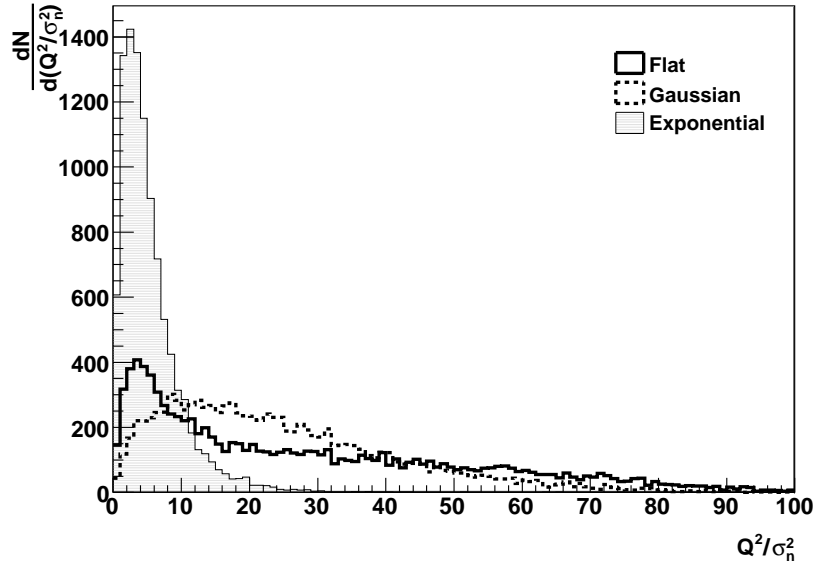


Fig. 6. Quality factor distributions for the different signal amplitudes, as obtained when using imperfect OFC's (i.e. computed from the predicted ionization pulse  $\mathbf{g}$  for non null residuals  $\mathbf{r}$ ).

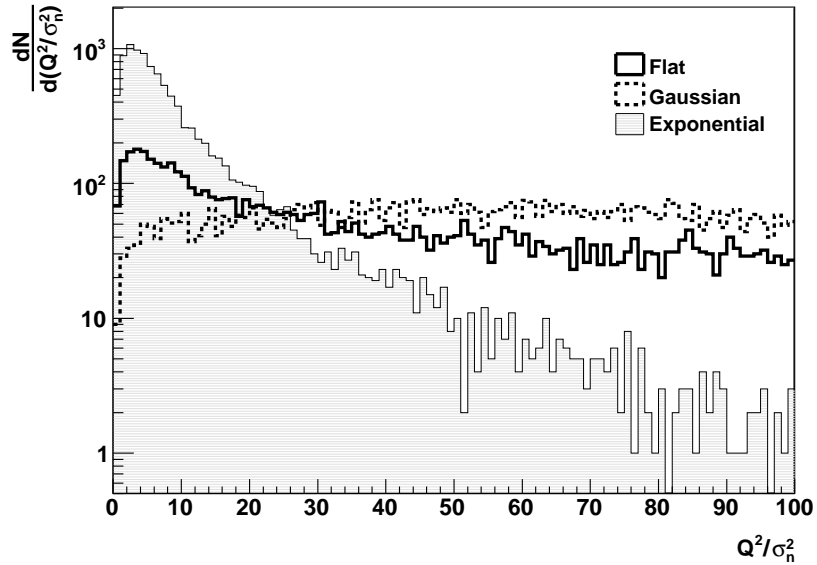


Fig. 7. Quality factor distributions obtained using perfect OFC's for signals out-of-time by  $\sim 1$  ns.

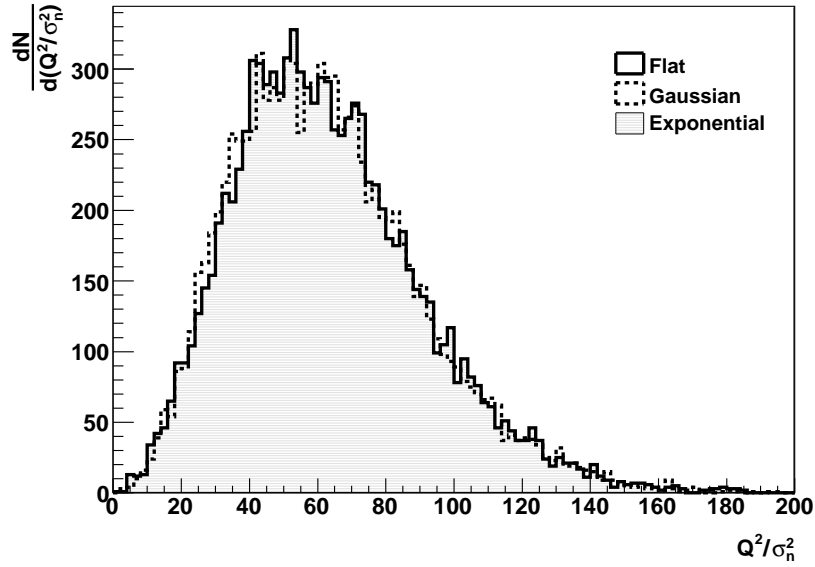


Fig. 8. Quality factor distributions obtained using perfect OFC's for signals affected by noise bursts. The noise bursts are simulated by summing a noise spike – normally generated with a  $4\sigma_n$  mean and  $1\sigma_n$  RMS – to one signal sample at random, and subtracting it from the following sample.

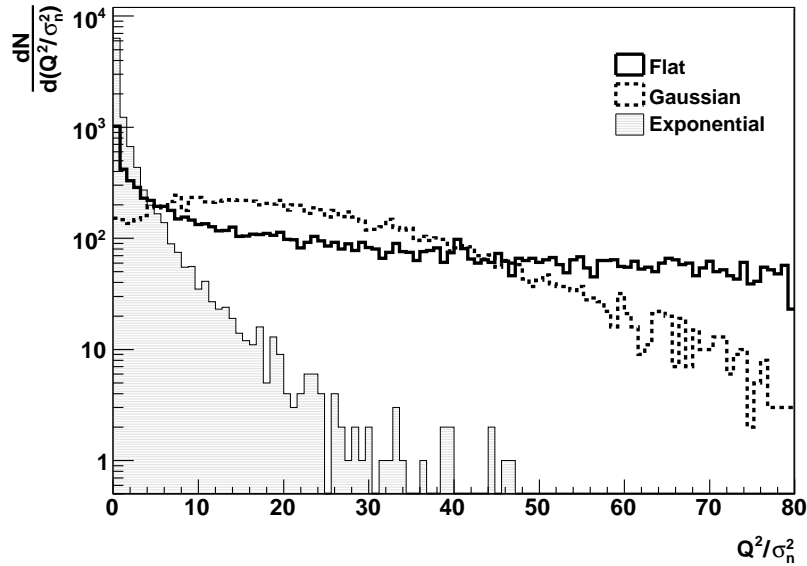


Fig. 9. Quality factor distributions obtained using perfect OFC's for signals affected by large capacitive cross-talk from neighbor cells. The cross-talk distortion is simulated by summing to the current pulse with one having the shape of the signal derivative  $\mathbf{h}'$ , and amplitude proportional to 1.5% of a signal independently generated from the same amplitude distribution.

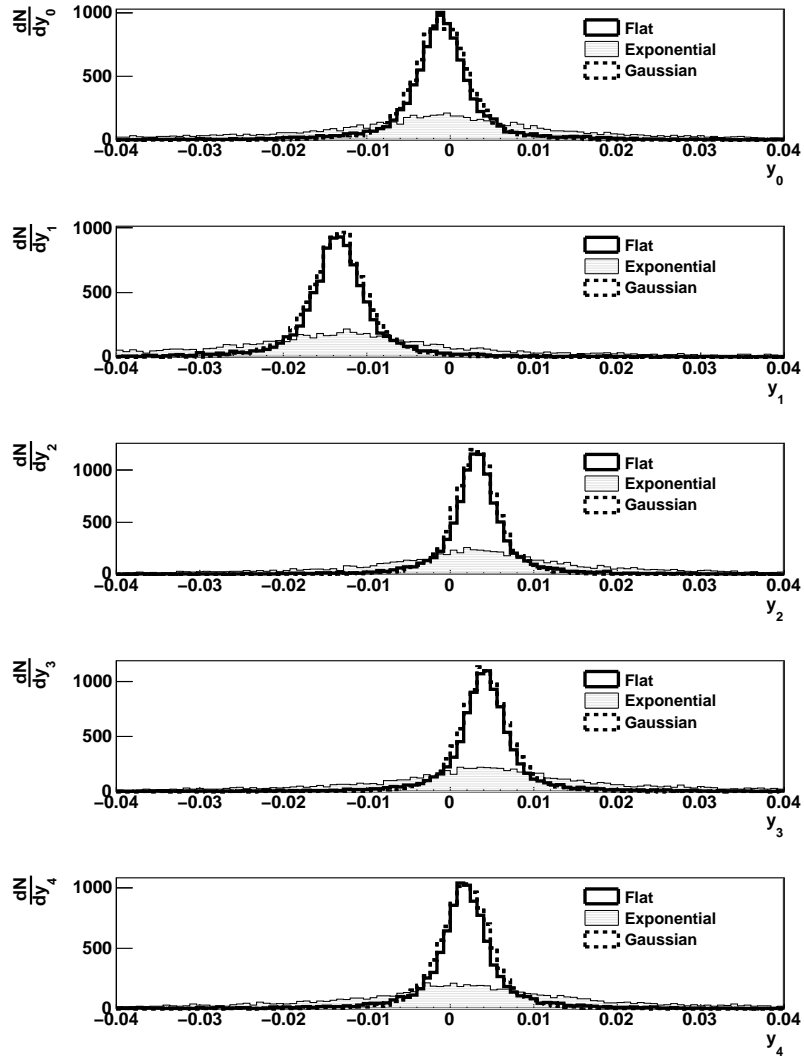


Fig. 10. Event pseudo-residual component distributions, as obtained for the different signal amplitudes for  $\hat{A} > 25 = 5\sigma_n$ .

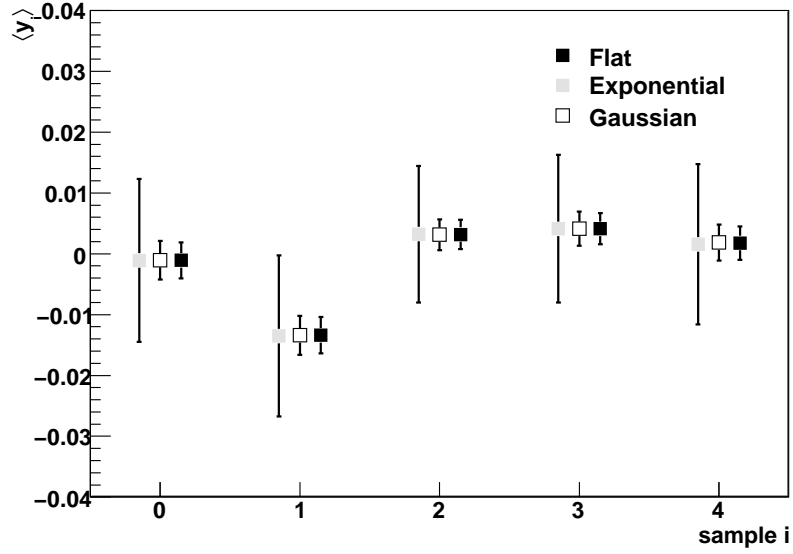


Fig. 11. Means of the event pseudo-residual component distributions for the different signal amplitude distribution  $P(A)$  and for  $\hat{A} > 25 = 5\sigma_n$ . Error bars indicate the widths of the distributions.

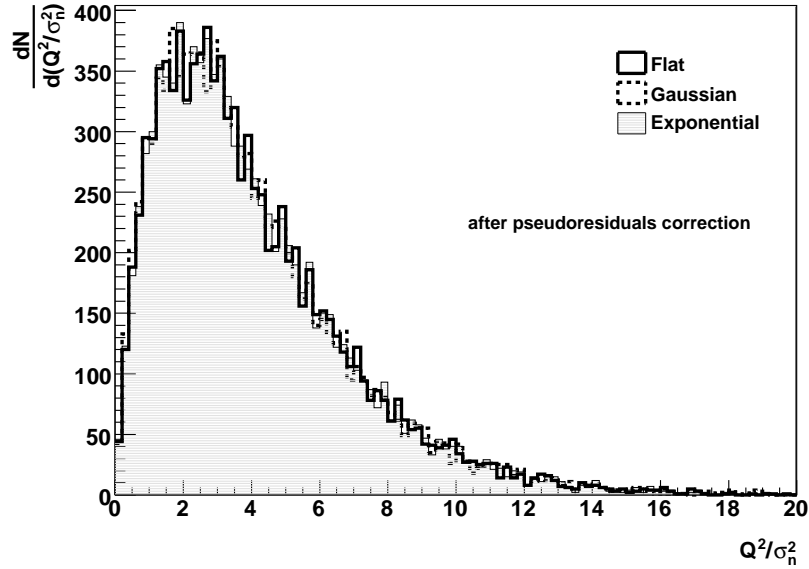


Fig. 12. Distributions of reconstructed amplitude relative error, as obtained when correcting the OFC's input pulse  $\mathbf{g}$  with the pseudo-residual estimators  $\langle \mathbf{y} \rangle$ .

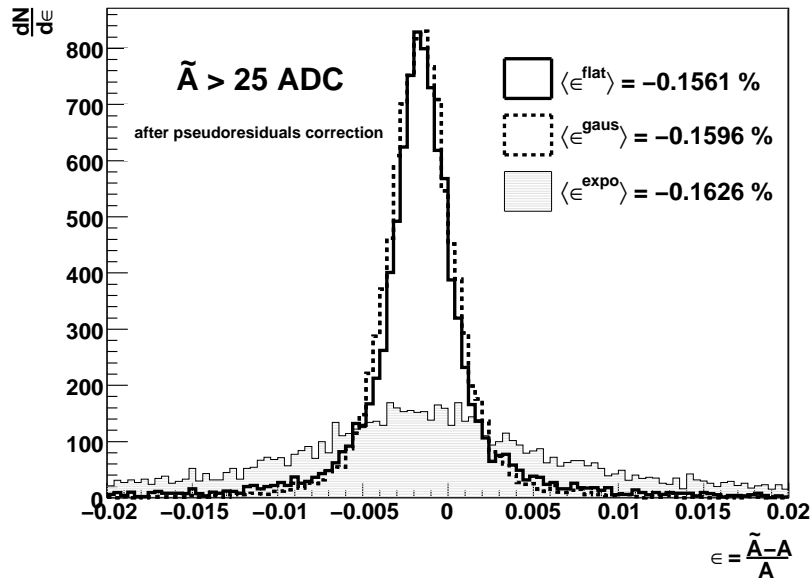


Fig. 13. Quality factor distributions for the different signal amplitudes, as obtained when correcting the OFC's input pulse  $\mathbf{g}$  with the pseudo-residual estimators  $\langle \mathbf{y} \rangle$ .

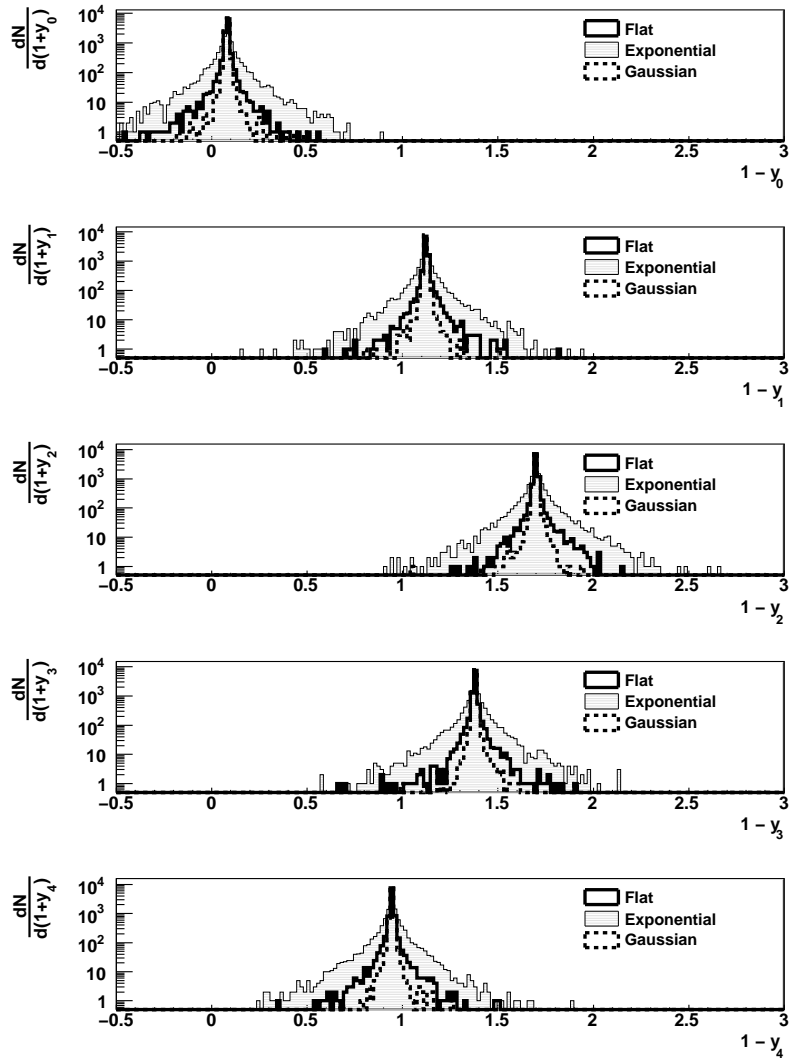


Fig. 14. Distributions of event pseudo-residual components biased by 1, as obtained for the different signal amplitudes for  $\tilde{A} > 25 = 5\sigma_n$ , when a flat filter is used for the amplitude reconstruction.

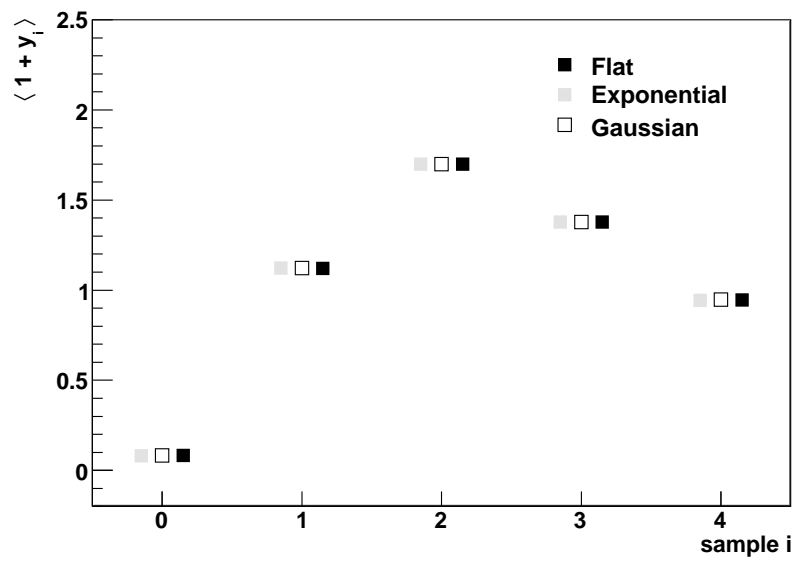


Fig. 15. Means of the distributions of the event pseudo-residual components biased by 1 for the different signal amplitude distribution  $P(A)$  and for  $\hat{A} > 25 = 5\sigma_n$ , when a flat filter is used for the amplitude reconstruction. The error bars are smaller than the point markers.